

# Geophysical Research Letters

## RESEARCH LETTER

10.1029/2020GL087774

### Key Points:

- We define critical volumes for fractures under the influence of a stress gradients that cause self-sustaining propagation
- We define such critical volumes analytically such that they are independent of scale. These are verified numerically
- The equation predicts the correct scale in natural and analog examples but for hydro-fracturing its too low

### Supporting Information:

- Supporting Information S1
- Data Set S1

### Correspondence to:

T. Davis,  
davis@gfz-potsdam.de

### Citation:

Davis, T., Rivalta, E., & Dahm, T. (2020). Critical fluid injection volumes for uncontrolled fracture ascent. *Geophysical Research Letters*, *47*, e2020GL087774. <https://doi.org/10.1029/2020GL087774>

Received 2 MAR 2020

Accepted 3 JUN 2020

Accepted article online 20 JUN 2020

## Critical Fluid Injection Volumes for Uncontrolled Fracture Ascent

Timothy Davis<sup>1</sup> , Eleonora Rivalta<sup>1</sup> , and Torsten Dahm<sup>1</sup> 

<sup>1</sup>GFZ (GeoForschungsZentrum), Physics of Earthquakes and Volcanoes, Potsdam, Germany

**Abstract** Hydrofracturing is a routine industrial technique whose safety depends on fractures remaining confined within the target rock volume. Both observations and theoretical models show that, if the fluid volume is larger than a critical value, pockets of fluid can propagate large distances in the Earth's crust in a self-sustained, uncontrolled manner. Existing models for such critical volumes are unsatisfactory; most are two-dimensional and depend on poorly constrained parameters (typically the fracture length). Here we derive both analytically and numerically in three-dimensional scale-independent critical volumes as a function of only rock and fluid properties. We apply our model to gas, water, and magma injections in laboratory, industrial, and natural settings, showing that our critical volumes are consistent with observations and can be used as conservative estimates. We discuss competing mechanisms promoting fracture arrest, whose quantitative study could help to assess more comprehensively the safety of hydrofracturing operations.

**Plain Language Summary** Fractures in rocks can act as channels for fluids. Fracking, or hydrofracturing, involves injection of fluids at high pressure in order to grow fractures within the rock and increase its permeability. Fluid volumes need to be kept below a threshold value: If the fluid volume is larger, then the stresses at the tips of the fluid pocket will be large enough for the fluids to force their way around by fracturing the rock ahead of them. Previous theoretical models for the critical volumes are unsatisfactory as they are two-dimensional and based on poorly constrained parameters. We derive and test a new three-dimensional equation that uses only rock and fluid parameters. We find that typical volumes injected in hydrofracturing operations are over the limit we define. We argue they are still mostly safe as additional processes often hinder fracture growth. Further work is needed to comprehensively quantify mechanisms that hinder hydrofracture arrest.

## 1. Introduction

Official guidelines for hydraulic fracturing (e.g., EPA, 2016; Mair et al., 2012) outline safe operational practices for regulators. Such reports often state that during routine operations, fractures are unlikely to grow out of the target rock formation, as typical injection pressures are too low for this to occur. These claims are substantiated with empirical observations from closed access microseismic data of scarce vertical fracture growth following injection (Fisher & Warpinski, 2012). Evidence for unsafe vertical migration of such fluids remains ambiguous (Vidic et al., 2013).

Natural analogs of fluid migration by hydrofracturing include drainage crevasses in melting glaciers and magma transport by diking. Field and experimental observations provide some indication of typical rates of fracture ascent, in the order of mm/s to around half a m/s (Das et al., 2008; Tolstoy et al., 2006). For water-filled fractures in rock, this has not been observed; estimates from geochemical analysis supply similar rates of ~0.01–0.1 m/s (1 km/day) (Okamoto & Tsuchiya, 2009). Theoretical arguments suggest that the migration velocity should have a dependency on volume (Dahm, 2000; Heimpel & Olson, 1994).

According to theory, tip-propagation occurs when a critical amount of fluid has accumulated, inducing enough stress to overcome the medium's fracture toughness,  $K_c$  (Secor & Pollard, 1975). So far, critical “volumes” are given in terms of the fracture length, which is not directly observable and difficult to estimate from observations (Dahm, 2000; Secor & Pollard, 1975; Taisne et al., 2011); moreover, such analyses have been carried out in 2-D only, not capturing the fracture's 3-D shape and scaling of volume versus length.

©2020. The Authors.

This is an open access article under the terms of the Creative Commons Attribution License, which permits use, distribution and reproduction in any medium, provided the original work is properly cited.

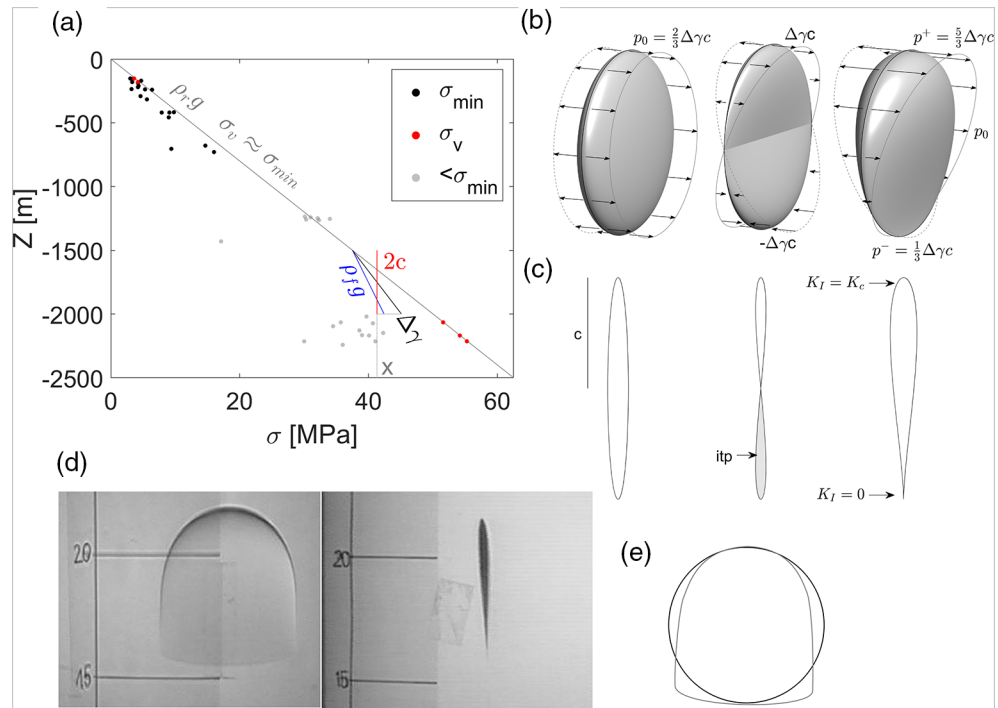


**Figure 1.** (a) Stress versus depth in the crust; data from Bell et al. (1990). Crack shown in red with length  $2c$ . (b) Stress boundary conditions and 3-D crack wall displacement. (c) Cross sections of crack wall displacement, itp = interpenetration. (d) Shape of an ascending air-filled crack in gelatine from Rivalta and Dahm (2006). (e) Air-filled cracks tipline versus a penny-shaped tipline.

Here, after deriving a theoretical model and validating it with numerical simulations, we apply this to cracks filled with air, water, oil, and magma in solids of varying stiffness and toughness, across a wide range of length scales.

## 2. Methods

### 2.1. Hydrofracturing and Stress Gradients

We consider a pressurized penny-shaped crack of radius  $c$  and volume  $V$  in an elastic medium. The crack can only grow when the stress intensity  $K_I$  at its tipline exceeds  $K_c$ . The elastic parameters of the medium (shear modulus,  $\mu$ , and Poisson's ratio,  $\nu$ ) control the fracture's aperture. The internal pressure  $p_0$  must overcome the stress normal to the crack walls (generally the minimum compressive stress,  $\sigma_{min}$ ) by an amount accommodating the volume  $V$  against the elastic forces (Figures 1a and 1b).

When the crack is vertical, the gradient in the normal stress acting to close the crack and the gradient in the load due to the overlying fluid acting to open the crack, that is,  $\rho_r g$  and  $\rho_f g$  in Figure 1a, where  $\rho_r$  and  $\rho_f$  are the densities of the host rock and fluid, respectively, result in a net stress gradient  $\Delta\gamma$  acting to push open the crack walls in an inverse “teardrop” shape (Figures 1b and 1c). When the crack is inclined,  $\Delta\gamma$  needs to be adjusted by  $\cos(\theta)$ , where  $\theta$  is the cracks' angle away from vertical. Quantitative formulations used to assess industrial fracture heights neglect stress gradients (e.g., Xu et al., 2019; Yue et al., 2019). This contrasts with routine observations of stress gradients from industry data (Figure 1a) and the fact that these gradients are considered in the well design of industrial operations (Lecampion et al., 2013; Mair et al., 2012). When this gradient is included in formulations, stress intensity varies around the fracture's tipline (Figure 2). Where  $K_c$  is exceeded, the upper tipline advances. The contained fluid flows into this newly created fracture surface while the bottom edge of the fracture is pinched shut as the internal pressure drops. With a great enough volume, this fluid movement maintains a critically stressed upper tipline, and the fracture reaches a state of “self-sustaining propagation.” Fluid viscosity will cause some fluid to stay trapped in the tail trailing

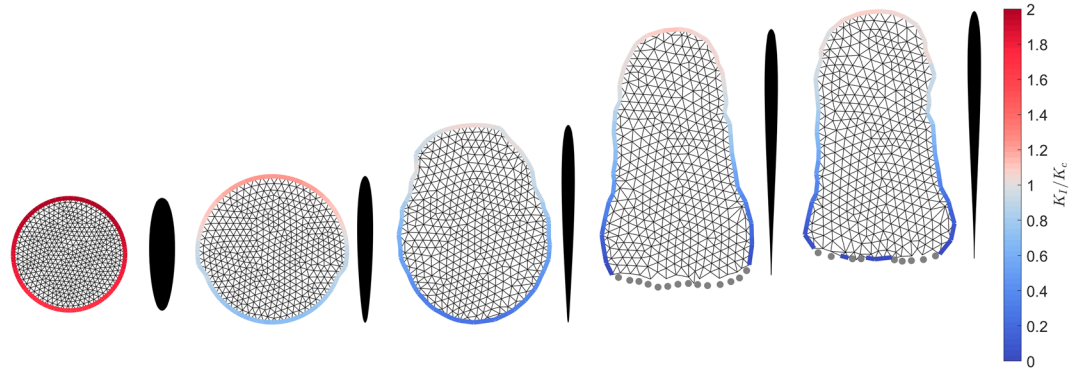


**Figure 2.** Numerical simulation of crack propagation (from left to right), looking at the fractures' face (left) and cross section (right). Gray points are edges that closed in the previous iteration.

behind the fracture; if fluid viscosity is low enough, the contained fluid is virtually all transported. Provided the fracture's shape and volume are maintained, no additional forces, such as pressure from injection, are required to aid this state of propagation.

## 2.2. Analytical Formulation

Secor and Pollard (1975) define in 2-D the size and pressure inside a vertical fracture subject to  $\Delta\gamma = (\rho_r - \rho_f)g$  such that at the upper tip,  $K_I^+ = K_c$ , and at the lower tip,  $K_I^- = 0$ . We derive an analytical expression for the fluid volume needed for a 3-D crack to propagate in a self-sustained manner.

$K_I$  for a Mode I penny-shaped fracture of radius  $c$  subject to a generic linear stress gradient can be expressed as the superposition of  $K_I$  for a penny-shaped fracture subject to a uniform pressure  $p_0$ :

$$K_I = \frac{2}{\pi} p_0 \sqrt{\pi c} \quad (1)$$

and that for a penny-shaped fracture subject to a linear pressure gradient  $\Delta\gamma$  where pressure is equal to 0 at the fracture's midpoint (Tada et al., 2000, p. 355):

$$K_I^\pm = \pm \frac{4}{3\pi} \Delta\gamma c \sqrt{\pi c} \quad (2)$$

where + refers to the propagating tip and - to the basal tip. Requiring  $K_I^- = 0$  results in  $p_0 = 2\Delta\gamma c/3$  and thus

$$p^\pm = \left( \frac{2}{3} \pm 1 \right) \Delta\gamma c \quad (3)$$

Requiring  $K_I^+ = K_c$  and rearranging for  $c$  yields

$$c = \left( \frac{3\sqrt{\pi}K_c}{8\Delta\gamma} \right)^{2/3} \quad (4)$$

We note that the 2-D plane strain critical length is  $\approx 0.9c$ . The volume of the crack can be calculated based on the equation for a crack pressurized by uniform pressure  $p_0$ , as the antisymmetric pressure contribution integrates to zero. Thus using (Tada et al., 2000),

$$V = \frac{8(1-\nu)}{3\mu} p_0 c^3 \quad (5)$$

results in

$$V_c^{an} = \frac{(1-\nu)}{16\mu} \left( \frac{9\pi^4 K_c^8}{\cos(\theta)\Delta\gamma^5} \right)^{1/3} \quad (6)$$

This equation requires validation in order to evaluate the bias due to approximating the shape of the propagating crack as circular (Figures 1d and 1e).

### 2.3. Numerical Model

To simulate propagation, we use a 3-D Boundary Element program where each element is a triangular dislocation with constant displacement (Figure 2) (Nikkhoo & Walter, 2015). The program computes fracture opening and stress intensities, based on fracture shape, rock and fluid parameters, and external stresses Davis et al. (2019). Our workflow during each iteration is as follows:

1. We invert for the uniform internal fluid pressure,  $p_0$ , necessary to open the crack to match the required volume against all external and internal tractions. Nonlinear complementarity conditions are imposed such that the crack's faces cannot interpenetrate (Davis et al., 2019).
2. We calculate the crack opening and the stress intensity at the tipline using the method of Davis et al. (2019). In order to reduce artifacts, we smooth the stress intensity along the tipline by averaging the local  $K_I$  with its two neighboring edges.
3. We calculate the advance or retreat of the tipline. At elements where  $K_I$  exceeds  $K_c$ , the tipline will advance proportionally to  $K_I/K_c$ . This approximation is akin to the "Paris fatigue law" (Lecampion et al., 2018). The maximum crack advance will occur at the triangle where  $K_I$  is maximum; this advance is set equal to the mesh's average triangle size. The triangular elements that close are removed. The simulation assumes the fluid is inviscid, and, as such, we cannot retrieve time-dependent propagation rates.
4. Once the fracture's edge has been updated, it is remeshed and cleaned such that the triangles on the fractures tipline are approximately equal size and isosceles (Da & Cohen-Steiner, 2019).

For a description of the numerical methods accuracy, see Appendix A1. We start the simulation with a vertical penny-shaped crack. We fix the number of elements,  $K_c$ ,  $\Delta\gamma$ ,  $\mu$ ,  $\nu$ , and the volume of fluid,  $V$ . We set the initial radius to  $0.4c$  (Equation 4). In our 350+ simulations, we use variables spanning several orders of magnitude:  $G = 190\text{--}5\cdot 10^{10}$  Pa,  $\nu = 0.25\text{--}0.49$ ,  $\Delta\gamma = 7.8\cdot 10^2\text{--}2.2\cdot 10^4$  Pa·m<sup>-1</sup>, and  $K_c = 1\text{--}1\cdot 10^8$  Pa·m<sup>0.5</sup>. We state the fracture has reached self-sustaining ascent when its upper tip has traveled  $4c$  upwards.

For all simulations, independent of mesh sampling, we find that if  $V=0.7V_c^{an}$ , the numerical code returns a trapped fracture, and if  $V=0.8V_c^{an}$ , the fracture always reaches self-sustaining propagation. Therefore, scaling Equation 6 by 0.75 supplies the numerical estimate of  $V_c$ , independent of the scale we use:

$$V_c^{num} = 0.75 \frac{(1-\nu)}{16\mu} \left( \frac{9\pi^4 K_c^8}{\cos(\theta)\Delta\gamma^5} \right)^{1/3} \quad (7)$$

For all cracks that reached self-sustaining propagation, the horizontal and vertical lengths were greater than  $\sim 0.6c$  and  $\sim 1.14c$ , respectively.

## 3. Applications

### 3.1. Analog Gelatine Experiments

The analog study of Heimpel and Olson (1994) inspects critical volumes of fluids ascending in gelatine blocks of different stiffness and fracture toughness (Figure 3). The graph of volume versus speed from their experimental results shows a rapid increase in speed past a certain volume. The authors interpret that at velocities past  $\sim 0.7$  cm/s (crosses in Figure 3), the ascent transitions from a subcritical propagation regime

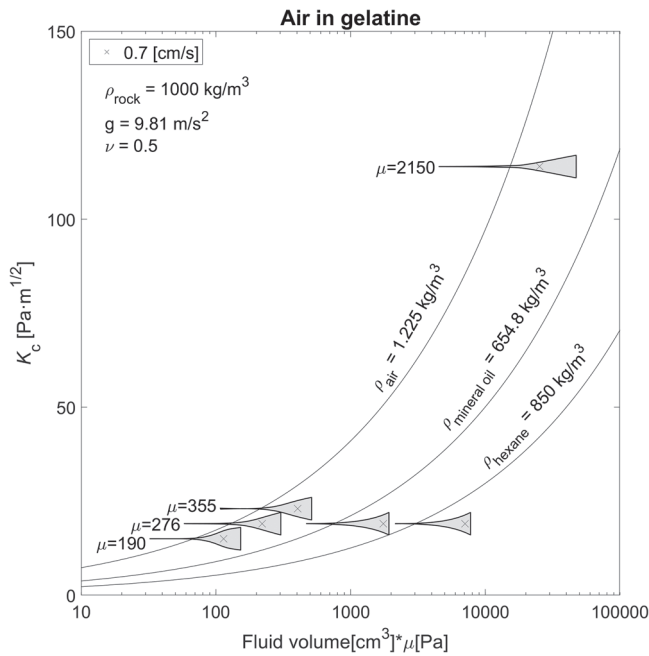


**Figure 3.**  $V^*\mu$  versus  $K_c$  from Heimpel and Olson (1994). Equation 7 predictions shown as black lines. The thickness of the gray filled patches represents the velocity of the crack as the volume increases, normalized by maximum observed velocity.

( $K_f < K_c$ ), where the fracture growth speed at the tip limits the velocity (Atkinson & Meredith, 1987) to a dynamic propagation regime. We test if our equation can predict volume of fluid that causes this transition in ascent speed. As Heimpel and Olson (1994) estimate  $K_c$  directly from this change in velocity, to verify that we can use this estimation, we calculate  $K_c$  differently, directly from the measured value of  $G$ . Strain energy release  $\mathcal{E}$  increases with greater stiffness in gelatin solids:  $\mathcal{E}[\text{N/m}] \approx 6.66 \cdot 10^{-4} G$  [Pa] (Czerner et al., 2016). This second independent estimate of  $K_c$  lies within  $5 \text{ Pa}\cdot\text{m}^{1/2}$  of the original estimate. Using  $\rho_r = 1,000 \text{ kg}\cdot\text{m}^{-3}$ ,  $\nu = 0.5$  and setting  $\mu$ ,  $\rho_f$ , and  $K_c$  to match the experiments of Heimpel and Olson (1994), we find that our value of  $V_c^{num}$  independently captures the point at which the velocity transitions, described above, supporting the previous interpretation that this describes the transition to dynamic fracture propagation.

### 3.2. Magmatic Dikes

We consider magma propagation volumes at Piton de la Fournaise, La Réunion, to see how our equation matches observed dike volumes. The volumes of the dike intrusions observed between 1998 and 2016 range from  $0.05\text{--}3.2 \cdot 10^6 \cdot \text{m}^3$  (Froger et al., 2004; Fukushima et al., 2005, 2010; Smittarello et al., 2019). Using  $\rho_r - \rho_f = 100 \text{ kg}\cdot\text{m}^{-3}$ ,  $\mu = 5 \text{ GPa}$ ,  $\nu = 0.25$ , and  $K_c$  ranging from 29 to  $112 \text{ MPa}\cdot\text{m}^{1/2}$  (Delaney & Pollard, 1981; Fukushima et al., 2010), we retrieve  $V_c^{num} = 0.05 \cdot 10^6$  and  $2 \cdot 10^6 \cdot \text{m}^3$ , respectively. The critical volumes we estimate are consistent with the observed dike sizes. As such, our approximation predicts the correct scale

in natural settings, provided  $K_c$  values estimated from field data are used, noting such field values appear to correct due to a number of additional processes that we have disregarded, instead of being representative of the rock strength at the scale of a laboratory sample.

### 3.3. Water Injection Into Stiff Rock

The UK government defines hydraulic fracturing as operations that use over  $1,000 \text{ m}^3$  of fluid per frack stage. During a hydrofracturing procedure, proppant is injected in the final phase to maintain an open fracture (e.g., spherical quartz grains). After the operation, not all injected fluid is recovered when the wellhead valve is opened: Vidic et al. (2013) report an average of only 10% fluid recovery in flowback waters, noting that this recovery volume decreases when shut-in times are longer. Using  $\rho_r = 2,700 \text{ kg}\cdot\text{m}^{-3}$ ,  $\rho_f = 1,000 \text{ kg}\cdot\text{m}^{-3}$ ,  $\mu = 8.9 \text{ GPa}$ ,  $\nu = 0.25$ , and  $K_c$  in the range  $0.36\text{--}4.05$  to  $7\text{--}25 \text{ MPa}\cdot\text{m}^{1/2}$ , we obtain  $V_c^{num} = 6 \cdot 10^{-2}$  and  $500 \text{ m}^3$ , respectively. These  $K_c$  values are for laboratory-sized shale samples from 100 to  $1,000 \text{ m}$  confining pressure and effective  $K_c$  values estimated for veins in the field, respectively (Gehne et al., 2020; Olson, 2003). Current operations use volumes around double our highest predicted limit. Few observations attest to the fact that industrial operations can cause ascent of fluids in fractures. One such example is the spectacular surface fissures created due to steam injection documented in Schultz (2016); additional examples can be found in Schultz et al. (2016). Geochemical data from aquifers above fracking operation sites have shown some evidence of the contamination of overlying units, which is attributed to poor well casing design, rather than fracture ascent (Vidic et al., 2013). Usually, microseismic monitoring of actual fracking operations show limited vertical extents of the fractures; however, these data are proprietary, and methodological descriptions are scarce (Fisher & Warpinski, 2012). Experimental fracturing data are of little help as volumes injected are typically below or close to our volumetric limit, with injected volumes of 2 to  $20 \text{ m}^3$  (Pandurangan et al., 2016; Warpinski et al., 1982).

Natural degassing, such as  $\text{CO}_2$  in the Cheb Basin, Czech Republic, has chemical signatures of fluids that have ascended over  $20 \text{ km}$  through the crust (Weinlich, 2014). Fracture-driven ascent can explain this phenomena without the requirement of permanent highly conductive fluid pathways at great depths. Supercritical  $\text{CO}_2$  at depth has a similar density to water and as such may be a good natural analog for water-filled fracture ascent. We saw that in analog and magmatic examples, Equation 7 predicts the

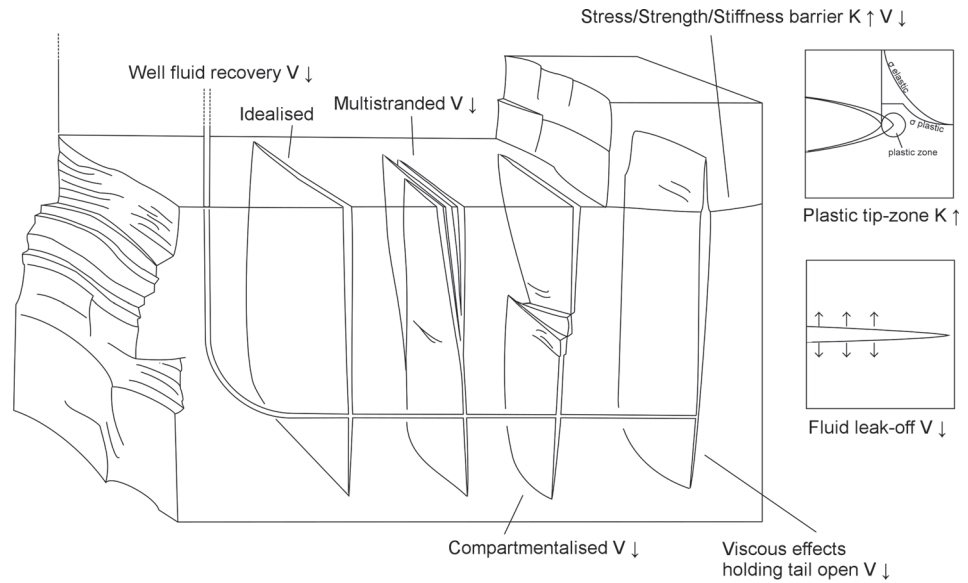


**Figure 4.** Processes that can hinder fracture ascent;  $K$  and  $V$  relate to effective  $K_c$  and  $V_c$  operating in Equation 7.

correct order of magnitude of critical volumes; at the same time, it appears that this equation is conservative for high volume water injection as fracture ascent in these settings has rarely been observed.

#### 4. Discussion and Conclusions

In summary, Equation 7 provides an estimate of the minimum fluid volume for self-sustained propagation of fluid-filled fractures, ranging from cm to tens of km.  $V_c$  is dependent on  $K_c^{8/3}$ ; since  $K_c$  is often poorly constrained,  $V_c$  suffers from large uncertainties. Values of  $K_c$  obtained in laboratory experiments show a strong dependency on pressure and temperature. Field estimates of effective  $K_c$  from trapped fractures can be orders of magnitude larger. An effective way to estimate  $K_c$  in Equation 7 incorporating all processes affecting the energy needed to extend the fracture at different scales would clearly be beneficial for any fracture-mechanics-based analysis of rock masses and the resultant interpretations.

In our derivation, we have neglected the effects of viscosity. Whether these effects will dominate over toughness in determining fracture growth can be assessed by evaluating the time scale needed for the fluid pressure to equilibrate within the crack, as this will mean that viscous dissipation is low and crack growth will be toughness dominated (Bunger & Detournay, 2007). The model of Bunger and Detournay (2007) assumes a constant injection rate with no stress gradients; we assume this still provides a rough estimate of the time scale until this transition. Typical industrial operations use fluid viscosity of 0.001–0.01 Pa·s, injection rates between 0.5 and 10 m<sup>3</sup>/min, and stiffnesses of 10–40 GPa. Using low values of  $K_c$  from laboratory experiments in shale, 0.36 MPa·m<sup>1/2</sup>, this transition time ranges between 1 min and times exceeding the end of injection. On the other hand, setting  $K_c$  higher from values for shale at depth, for example, 4 MPa·m<sup>1/2</sup>, significantly reduces this range from milliseconds to a maximum of 5 hours. This suggests that, depending on  $K_c$ , Equation 7 can be a relevant estimate of  $V_c^{num}$ , independent of viscous forces.

While theory and experiments support Equation 7, this appears to be overly conservative in practice, as injections of quantities of fluid exceeding this do not result in significant ascent in most cases. In part, this discrepancy results from our simplification of the process as mass-conserving propagation in a homogeneous linear-elastic medium. Figure 4 shows a schematic of processes not quantified in relation to critical fluid volumes, which we review in detail below.

1. A series of mechanisms can reduce  $V$  during propagation and thus promote crack arrest. These include leak-off from the fractures faces, the fracture becoming multistranded/compartamentalized, fluid recovery (extraction), or fluid remaining in the tail of the fracture due to added proppant or viscous forces (Taisne & Tait, 2009).

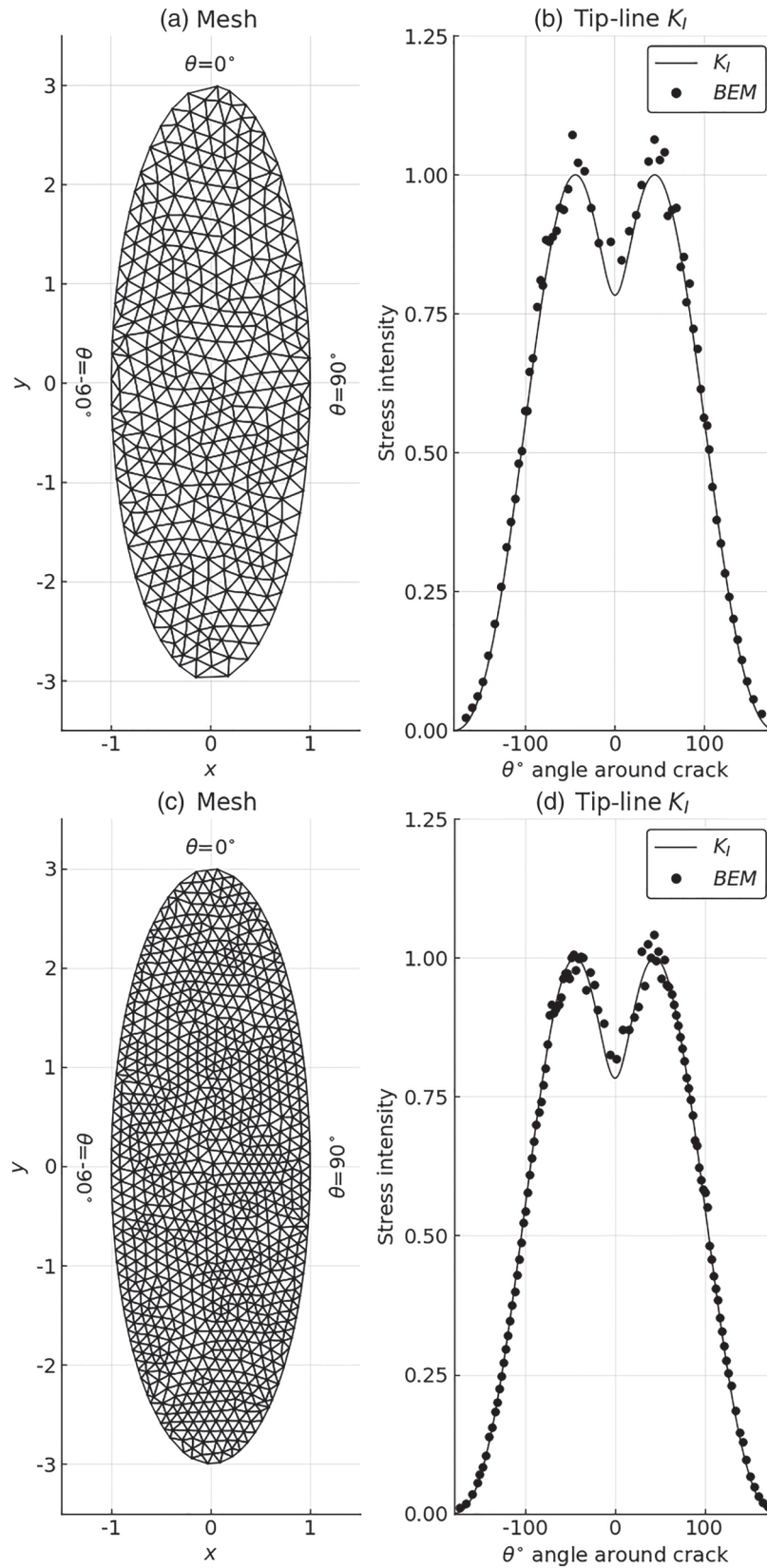


**Figure A1.** Stress intensity factor approximation using the 3-D displacement discontinuity method. (a, c) Elliptical crack meshed with 650 and 1,500 triangles, respectively, (b, d) Numerical (dots) and analytical (solid line) results. Results are normalized relative to the maximum analytical value of  $K_I$ .

2. Mechanisms that can lead to an effective increase of  $K_c$ , and thus also promote crack arrest, include plastic tip processes, the fracture entering in a zone of damage of the host rock (Kaya & Erdogan, 1980; Sih et al., 1965), or seismicity surrounding the fracture, causing reduction in the system's energy/blunting the fracture's tip (Rivalta et al., 2015).
3. Heterogeneous  $\mu$  or  $K_c$  or stress barriers may also lead to arrest of fractures by deflection or promoting lateral growth (Bunger & Lecampion, 2017; Maccaferri et al., 2011; Warpinski et al., 1985),
4. Equation 7 has a clear dependency on the fracture's dip. If the minimum compressive stress is vertical, this promotes flat-lying fractures.

Quantification of processes acting to halt fracture ascent, especially in the context of the variables in our equation, are critical to understand which volumetric limits can be deemed safe. In particular, the gradient in stress with depth must be included to assess this process. Without such quantification, regulation of this industrial process will continue to rely on empirical evidence for safe rates, volumes, and depths from select operations that may not be representative.

## Appendix A: Numerical

### A1. Numerical Accuracy

We verify that our method to compute  $K_I$  is independent of crack shape and boundary condition. Previously, this was only compared to solutions for a circular crack subject to uniform stresses (Davis et al., 2019). We compare this to the analytical solution for the stress intensity around an elliptical crack, subject to a superposition of uniform pressure and a linear gradient of stress such that, at the basal tip,  $K_I=0$  (Figure 1) (Atroshchenko et al., 2009). We note that under a stress gradient,  $K_I$  for vertically aligned elliptical cracks is not maximal at its upper tip, due to the reduction in crack surface area proximal to this edge.

For a mesh with 650 triangles (Figures A1a and A1b), the greatest vertical separation between the numerical points and the analytical line is 0.09. For this test, we required the edge points of the mesh's triangles, not the midpoints of the triangles edge where  $K_I$  is calculated, to lie on the tipline defined by the analytical solution. For a mesh with 1,500 triangles (Figures A1c and A1d), the maximum vertical distance from the analytical solution is 0.06, noting that greater sampling does not necessarily converge to an improved accuracy; see appendix of Davis et al. (2019).

As a further test of numerical accuracy, we compare how well the numerical method approximates the opening volume of a penny-shaped crack subject to tension (Tada et al., 2000). We find that a sampling of 650 triangles overestimates the volume by 5.2%; by increasing the triangle count to 1,500, this drops to 3.5%.

### Data Availability Statement

The code used for the numerical analysis of this study was the open-source code <https://doi.org/10.5281/zenodo.3694163> with an interface with the Computational Geometry Algorithms Library software (C++) for meshing.

### Acknowledgments

The authors would like to thank the reviewers Meredith Townsend and Dmitry Garagash for their insightful and constructive reviews of the manuscript. T. Davis is funded by the DFG-ICDP Grant RI 2782/3-1.

### References

- Atkinson, B. K., & Meredith, P. G. (1987). The theory of subcritical crack growth with applications to minerals and rocks. *Fracture Mechanics of Rock*, 2, 111–166.
- Atroshchenko, E., Potapenko, S., & Glinka, G. (2009). Stress intensity factor for an embedded elliptical crack under arbitrary normal loading. *International Journal of Fatigue*, 31(11-12), 1907–1910.
- Bell, J. S., Price, P. R., & McLellan, P. J. (1990). In-situ stress in the western Canada sedimentary basin. *Bulletin of Canadian Petroleum Geology*, 38(1), 157–157.
- Bunger, A., & Detournay, E. (2007). Early-time solution for a radial hydraulic fracture. *Journal of Engineering Mechanics*, 133(5), 534–540. [https://doi.org/10.1061/\(ASCE\)0733-9399\(2007\)133:5\(534\)](https://doi.org/10.1061/(ASCE)0733-9399(2007)133:5(534))
- Bunger, A. P., & Lecampion, B. (2017). Four critical issues for successful hydraulic fracturing applications. In X.-T. Feng (Ed.), *Rock mechanics and engineering* (Vol. 5, Surface and Underground Projects). CRC Press/Balkema. <https://doi.org/10.1201/9781315364223-16>
- Czerner, M., Fasce, L. A., Martucci, J. F., Ruseckaite, R., & Frontini, P. M. (2016). Deformation and fracture behavior of physical gelatin gel systems. *Food Hydrocolloids*, 60, 299–307.
- Da, T. K. F., & Cohen-Steiner, D. (2019). Advancing front surface reconstruction, (4.14.1). *CGAL user and reference manual*.
- Dahm, T. (2000). On the shape and velocity of fluid-filled fractures in the earth. *Geophysical Journal International*, 142(1), 181–192. <https://doi.org/10.1046/j.1365-246x.2000.00148.x>
- Das, S. B., Joughin, I., Behn, M. D., Howat, I. M., King, M. A., Lizarralde, D., & Bhatia, M. (2008). Fracture propagation to the base of the Greenland Ice Sheet during supraglacial lake drainage. *Science*, 320(5877), 778–781. <https://doi.org/10.1126/science.1153360>

- Davis, T., Healy, D., & Rivalta, E. (2019). Slip on wavy frictional faults: Is the 3rd dimension a sticking point? *Journal of Structural Geology*, *119*, 33–49. <https://doi.org/10.1016/j.jsg.2018.11.009>
- Delaney, P. T., & Pollard, D. D. (1981). *Deformation of host rocks and flow of magma during growth of minette dikes and breccia-bearing intrusions near ship rock*. New Mexico: USGPO. <https://doi.org/10.3133/pp1202>
- EPA, U. (2016). Hydraulic fracturing for oil and gas: Impacts from the hydraulic fracturing water cycle on drinking water resources in the United States. Washington, DC: US Environmental Protection Agency, EPA/600/R-16/236F.
- Fisher, M. K., & Warpinski, N. R. (2012). Hydraulic-fracture-height growth: Real data. *SPE Production & Operations*, *27*(01), 8–19. <https://doi.org/10.2118/145949-PA>
- Froger, J.-L., Fukushima, Y., Briole, P., Staudacher, T., Souriot, T., & Villeneuve, N. (2004). The deformation field of the August 2003 eruption at Piton de la Fournaise, Reunion Island, mapped by ASAR interferometry. *Geophysical Research Letters*, *31*, L14601. <https://doi.org/10.1029/2004GL020479>
- Fukushima, Y., Cayol, V., & Durand, P. (2005). Finding realistic dike models from interferometric synthetic aperture radar data: The February 2000 eruption at Piton de la Fournaise. *Journal of Geophysical Research*, *110*, B03206. <https://doi.org/10.1029/2004JB003268>
- Fukushima, Y., Cayol, V., Durand, P., & Massonnet, D. (2010). Evolution of magma conduits during the 1998–2000 eruptions of Piton de la Fournaise volcano, Réunion Island. *Journal of Geophysical Research*, *115*, B10204. <https://doi.org/10.1029/2009JB007023>
- Gehne, S., Forbes Inskip, N. D., Benson, P. M., Meredith, P. G., & Koor, N. (2020). Fluid-driven tensile fracture and fracture toughness in Nash point shale at elevated pressure. *Journal of Geophysical Research: Solid Earth*, *125*, e2019JB018971. <https://doi.org/10.1029/2019JB018971>
- Heimpel, M., & Olson, P. (1994). Buoyancy-driven fracture and magma transport through the lithosphere: Models and experiments, *International Geophysics* (Vol. 57, pp. 223–240): Elsevier.
- Kaya, A. C., & Erdogan, F. (1980). Stress intensity factors and COD in an orthotropic strip. *International Journal of Fracture*, *16*(2), 171–190. <https://doi.org/10.1007/BF00012620>
- Lecampion, B., Bunger, A., Kear, J., & Quesada, D. (2013). Interface debonding driven by fluid injection in a cased and cemented wellbore: Modeling and experiments. *International Journal of Greenhouse Gas Control*, *18*, 208–223. <https://doi.org/10.1016/j.ijggc.2013.07.012>
- Lecampion, B., Bunger, A., & Zhang, X. (2018). Numerical methods for hydraulic fracture propagation: A review of recent trends. *Journal of Natural Gas Science and Engineering*, *49*, 66–83. <https://doi.org/10.1016/j.jngse.2017.10.012>
- Maccafferri, F., Bonafede, M., & Rivalta, E. (2011). A quantitative study of the mechanisms governing dike propagation, dike arrest and sill formation. *Journal of Volcanology and Geothermal Research*, *208*(1–2), 39–50. <https://doi.org/10.1016/j.jvolgeores.2011.09.001>
- Mair, R., Bickle, M., Goodman, D., Koppelman, B., Roberts, J., Selley, R., et al. (2012). Shale gas extraction in the UK: A review of hydraulic fracturing.
- Nikkhoo, M., & Walter, T. R. (2015). Triangular dislocation: An analytical, artefact-free solution. *Geophysical Journal International*, *201*(2), 1119–1141. <https://doi.org/10.1093/gji/ggv035>
- Okamoto, A., & Tsuchiya, N. (2009). Velocity of vertical fluid ascent within vein-forming fractures. *Geology*, *37*(6), 563–566. <https://doi.org/10.1130/G25680A.1>
- Olson, J. E. (2003). Sublinear scaling of fracture aperture versus length: An exception or the rule? *Journal of Geophysical Research*, *108*(B9), 2413. <https://doi.org/10.1029/2001JB000419>
- Pandurangan, V., Chen, Z., & Jeffrey, R. G. (2016). Mapping hydraulic fractures from tiltmeter data using the ensemble Kalman filter. *International Journal for Numerical and Analytical Methods in Geomechanics*, *40*(4), 546–567. <https://doi.org/10.1002/nag.2415>
- Rivalta, E., & Dahm, T. (2006). Acceleration of buoyancy-driven fractures and magmatic dikes beneath the free surface. *Geophysical Journal International*, *166*(3), 1424–1439. <https://doi.org/10.1111/j.1365-246X.2006.02962.x>
- Rivalta, E., Taisne, B., Bunger, A. P., & Katz, R. F. (2015). A review of mechanical models of dike propagation: Schools of thought, results and future directions. *Tectonophysics*, *638*, 1–42. <https://doi.org/10.1016/j.tecto.2014.10.003>
- Schultz, R. A. (2016). Causes and mitigation strategies of surface hydrocarbon leaks at heavy-oil fields: Examples from Alberta and California. *Petroleum Geoscience*, *23*(2), 231–237. <https://doi.org/10.1144/petgeo2016-070>
- Schultz, R. A., Mutlu, U., & Bere, A. (2016). *Critical issues in subsurface integrity*. Paper presented at 50th US Rock Mechanics/Geomechanics Symposium, American Rock Mechanics Association.
- Secor, D. T., & Pollard, D. D. (1975). On the stability of open hydraulic fractures in the Earth's crust. *Geophysical Research Letters*, *2*(11), 510–513. <https://doi.org/10.1029/GL002i011p00510>
- Sih, G. C., Paris, P. C., & Irwin, G. R. (1965). On cracks in rectilinearly anisotropic bodies. *International Journal of Fracture Mechanics*, *1*(3), 189–203. <https://doi.org/10.1007/BF00186854>
- Smittarello, D., Cayol, V., Pinel, V., Peltier, A., Froger, J.-L., & Ferrazzini, V. (2019). Magma propagation at Piton de la Fournaise from joint inversion of InSAR and GNSS. *Journal of Geophysical Research: Solid Earth*, *124*, 1361–1387. <https://doi.org/10.1029/2018JB016856>
- Tada, H., Paris, P., & Irwin, G. (2000). *The stress analysis of cracks handbook* (3rd ed.). New York: ASME Press.
- Taisne, B., & Tait, S. (2009). Eruption versus intrusion? Arrest of propagation of constant volume, buoyant, liquid-filled cracks in an elastic, brittle host. *Journal of Geophysical Research*, *114*, B06202. <https://doi.org/10.1029/2009JB006297>
- Taisne, B., Tait, S., & Jaupart, C. (2011). Conditions for the arrest of a vertical propagating dyke. *Bulletin of Volcanology*, *73*(2), 191–204. <https://doi.org/10.1007/s00445-010-0440-1>
- Tolstoy, M., Cowen, J. P., Baker, E. T., Fornari, D. J., Rubin, K. H., Shank, T. M., et al. (2006). A sea-floor spreading event captured by seismometers. *Science*, *314*(5807), 1920–1922. <https://doi.org/10.1126/science.1133950>
- Vidic, R. D., Brantley, S. L., Vandenbossche, J. M., Yoxheimer, D., & Abad, J. D. (2013). Impact of shale gas development on regional water quality. *Science*, *340*(6134), 1235009. <https://doi.org/10.1126/science.1235009>
- Warpinski, N. R., Branagan, P., & Wilmer, R. (1985). In-situ stress measurements at US DOE's multiwell experiment site, Mesaverde Group, Rifle, Colorado. *Journal of Petroleum Technology*, *37*(03), 527–536. <https://doi.org/10.2118/12142-PA>
- Warpinski, N. R., Schmidt, R. A., & Northrop, D. A. (1982). In-situ stresses: The predominant influence on hydraulic fracture containment. *Journal of Petroleum Technology*, *34*(03), 653–664. <https://doi.org/10.2118/8932-PA>
- Weinlich, F. H. (2014). Carbon dioxide controlled earthquake distribution pattern in the NW Bohemian swarm earthquake region, western Eger Rift, Czech Republic—Gas migration in the crystalline basement. *Geofluids*, *14*(2), 143–159. <https://doi.org/10.1111/gfl.12058>
- Xu, W., Prioul, R., Berard, T., Weng, X., & Kresse, O. (2019). *Barriers to hydraulic fracture height growth: A new model for sliding interfaces*. Paper presented at SPE Hydraulic Fracturing Technology Conference and Exhibition, Society of Petroleum Engineers. <https://doi.org/10.2118/194327-MS>
- Yue, K., Olson J. E., & Schultz R. A. (2019). The effect of layered modulus on hydraulic-fracture modeling and fracture-height containment. *SPE Drilling & Completion*, *34*(04), 356–371. <https://doi.org/10.2118/195683-pa>